

Polyphosphate Adsorption and Hydrolysis on Aluminum Oxides

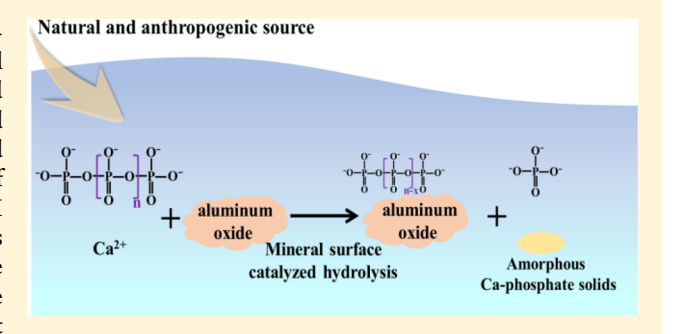
Biao Wan,[†] Rixiang Huang,[†] Julia M. Diaz,^{‡,§} and Yuanzhi Tang*,[†]

[†]School of Earth and Atmospheric Sciences, Georgia Institute of Technology, 311 Ferst Drive, Atlanta, Georgia 30332-0340, United States

[‡]Skidaway Institute of Oceanography, Department of Marine Sciences, University of Georgia, Savannah, Georgia 31411-1011, United States

Supporting Information

ABSTRACT: The geochemical behaviors of phosphate-containing species at mineral—water interfaces are of fundamental importance for controlling phosphorus mobility, fate, and bioavailability. This study investigates the sorption and hydrolysis of polyphosphate (a group of important long-chained phosphate molecules) on aluminum oxides in the presence of divalent metal cations (Ca²+, Cu²+, Mg²+, Mn²+, and Zn²+) at pH 6-8. γ -Al₂O₃ with three particle sizes (5, 35, and 70 nm) was used as an analogue of natural aluminum oxides to investigate the particle size effect. All metal cations enhanced polyphosphate hydrolysis at different levels, with Ca²+ showing the most



significant enhancement, and the difference in the enhancement might be due to the intrinsic affinity of metal cations to polyphosphate. In the presence of Ca²⁺, the hydrolysis rate decreased with increasing mineral particle size. Solid-state ³¹P nuclear magnetic resonance spectroscopy (NMR) revealed the main surface P species to be amorphous calcium phosphate precipitates, phosphate groups in polyphosphate that formed direct bonds with the mineral surface as inner-sphere complexes, and phosphate groups in polyphosphate that were not directly bonded to the mineral surfaces. Our results reveal the critical roles of mineral—water interface processes and divalent metal cations on controlling polyphosphate speciation and transformation and phosphorus cycling.

1. INTRODUCTION

Phosphorus (P) is as an essential nutrient for all living organisms and commonly exists as diverse phosphatecontaining molecules in natural environments. Polyphosphate is a group of important phosphate-containing species, composed of at least three phosphate ions joint by phosphoanhydride (P-O-P) bonds. Polyphosphates are synthesized by all living organisms and serve many important biological functions, such as ATP substitute, energy source, regulator for P stress and survival, and life evolution.^{2,3} Polyphosphates can be extracellular or intracellular. During common cell events, such as extracellular release, lysis, death, and burial of microorganisms, polyphosphates are released into various natural environments.⁴ For example, polyphosphates are found to represent 1-13% of total P in planktonic organisms, ^{2,5} the dissolved and particulate pools of seawater, ^{6,7} and marine sediments,8 as well as 0.4-7% of total P in soils.9 Polyphosphates are also important industrial chemicals, frequently used as reagents for water treatment, medicine, fertilizers, flame retardants, and food additives. 10 The widespread anthropogenic application of polyphosphates can ultimately result in their release into soils, water bodies, and sediments. Thus, understanding polyphosphate transport and transformation in natural environments has important implications for both geological and anthropogenic P cycles.

In soils and sediments, phosphate groups can strongly adsorb onto metal (hydr)oxides, and the sorption behavior depends on phosphate concentration, mineral type, pH, ionic strength, and the presence of competing or complexing ions. I1-13 Since the sorption of phosphate groups at mineral-water interfaces can significantly impact P distribution, mobility, transformation, and bioavailability, detailed understanding on the interaction between phosphate groupcontaining molecules and common minerals is needed to evaluate the interfacial behavior and bioavailability of P in aquatic and terrestrial environments. 14 Yet, very few studies have examined the chemical behaviors of polyphosphate at the mineral-water interface. Tripolyphosphate was reported to adsorb on aluminum (Al) hydroxide by forming monodentate binuclear inner-sphere complexes. 15 Tripolyphosphate was also found to hydrolyze on the surface of manganese oxides, which was enhanced in the presence of Ca²⁺ and Mg²⁺ ions. ¹⁶ Thus, it is likely that both adsorption and hydrolysis of polyphosphate on mineral surfaces can significantly affect its fate and transport at the mineral-water interface.

Received: March 28, 2019 Revised: June 25, 2019 Accepted: July 17, 2019 Published: July 17, 2019



Al (oxyhydr)oxides, such as amorphous Al hydroxides, boehmite, and gibbsite, are among the most abundant and reactive minerals found in natural environments, and are commonly considered as a critical metal oxide group (along with Fe and Mn oxides) that can significantly affect the environmental behaviors of numerous trace elements and contaminants. It is commonly accepted that mineral surface properties can significantly affect their reactivity during interfacial biogeochemical reactions. Thus, during the interaction of phosphate-containing molecules (such as polyphosphate) with minerals (via processes such as sorption and hydrolysis), mineral surface properties such as surface reactive sites, surface area, and particle size are likely to play key roles in determining the surface speciation and hydrolysis rate and extent.

In this study, we systematically characterized the uptake and hydrolysis kinetics and mechanisms of polyphosphate on Al oxide minerals under varied solution chemistry, such as pH and metal cation presence. γ -Al₂O₃ is an analogue to naturally occurring aluminum (oxy)hydroxides and Al-rich clay minerals, and is a well characterized phase that has been used to represent natural Al oxide minerals for numerous studies on the sorption of nutrients and metals (e.g., P, Zn, and other metals).^{17–21} It is commercially available in different particle sizes,¹⁷ allowing examination of the particle size effect. Compared to environmental Al oxide minerals (e.g., corundum, boehmite, gibbsite, and bayerite), γ-Al₂O₃ has higher surface area and reactivity for P adsorption.¹ Additionally, since γ-Al₂O₃ is not a paramagnetic mineral substrate (as compared to Fe/Mn minerals), solid-state ³¹P nuclear magnetic resonance (NMR) spectroscopy has been successfully applied to systematically characterize surface P species and reaction mechanisms during their interaction with aluminum (oxy)hydroxides. 17,21 Batch experiments were conducted to determine the hydrolysis rate and extent of polyphosphate by γ -Al₂O₃ with three different sizes (5, 35, and 70 nm), at varied pH (6 and 8), and in the presence of common divalent metal cations (Ca2+, Mg2+, Cu2+, Zn2+, Mn²⁺). Solution and solid-state ³¹P NMR spectroscopy analyses were conducted to reveal the hydrolysis mechanism and reaction products in both solid and solution phases. P Kedge X-ray absorption near edge structure (XANES) spectroscopy was used to identify the phase composition of the solid reaction products. Results from this study provide new insights for the abiotic transformation of polyphosphate and the formation mechanisms of calcium phosphate minerals at environmental interfaces. The results also lay the foundation for better understanding the geochemical processes controlling phosphorus transport and transformation in natural environ-

2. EXPERIMENTAL PROCEDURES

2.1. Materials and Characterization. Polyphosphate sodium salt with an average chain length of 10 (hereafter referred to as P_{10}) was purchased from Sigma-Aldrich. Three γ -Al $_2$ O $_3$ samples with different average particle sizes were used, including a 5 nm sample (Sky Spring Nanomaterials Inc., catalog no. 1328QI), 35 nm sample (Sigma–Aldrich, catalog no. 544833), and 70 nm sample (Alfa Aesar, catalog no. 43266). Details on sodium polyphosphate salt and γ -Al $_2$ O $_3$ samples are available in the Supporting Information Text S1 and Text S2.

2.2. Hydrolysis of Polyphosphate by Aluminum Oxides. Two sets of experiments were designed to explore the effects of γ -Al₂O₃ particle size, pH, and metal cations on polyphosphate hydrolysis at room temperature, as detailed below and summarized in Table S1.

Experiment Set I examined the effects of γ-Al₂O₃ particle size (5, 35, 70 nm), pH (6.0 vs 8.0), and presence/absence of Ca²⁺. This set of experiments used polyphosphate concentration of 2 mM (as total P), with/without 1 mM Ca²⁺, and 0.4 g L⁻¹ γ-Al₂O₃. Prior to the adsorption and hydrolysis experiments, 0.04 g of γ -Al₂O₃ (5, 35, 70 nm) and 0.58 g of NaCl (to achieve final background electrolyte strength of 0.1 M) were mixed in 95 mL of deionized water in a glass bottle and equilibrated overnight under magnetic stirring at 7 Hz. For experiments exploring the effects of Ca²⁺ on polyphosphate adsorption and hydrolysis, 2 mL of a stock solution of CaCl₂ (50 mM) was first added to 93 mL of deionized water before the addition of γ -Al₂O₃ and NaCl solids, in order to achieve a final Ca²⁺ concentration of 1 mM. pH of the suspension was manually adjusted to 6 ± 0.05 or 8.0 ± 0.05 using 0.05 M HCl and NaOH. After overnight equilibration, 5 mL of polyphosphate stock solution (with ~40 mM in total P concentration) was added into the suspension, in order to achieve a final polyphosphate concentration of 2 mM (as total P). The suspension pH was immediately readjusted. After this initiation of reaction, the pH of the reaction suspension was adjusted several times within the first 2 h, then at 3, 5, 7, 10, 24, 48, 72, 96, 168, and 216 h. At specific time points, aliquots (2 mL) of the suspension was filtered (0.22-μm Millipore membrane) and the supernatant analyzed for the concentrations of orthophosphate and total P. For total P analysis, all P in the supernatant was hydrolyzed to inorganic orthophosphate via potassium persulfate autoclave digestion,²² and orthophosphate concentration was determined using the phosphomolybdate colorimetric assay²³ on an UV-vis spectrometer (Carey 60, Agilent).

Experiment Set II was designed to compare the effects of different divalent metal cations (Ca2+, Mg2+, Cu2+, Zn2+, and Mn²⁺) on polyphosphate hydrolysis. This set of experiments used decreased concentrations of polyphosphate (1 mM as total P), metal cations (0.5 mM), and 5 nm γ -Al₂O₃ (0.1 g L^{-1}), and the purpose was to minimize direct precipitation of metal-polyphosphate solids, which may affect the mineralcatalyzed hydrolysis process. Specifically, a calculated amount (1 mL) of metal chloride stock solution (50 mM) was added into 96.5 mL of deionized water to reach the desired final metal concentration of 0.5 mM, then 0.01 g of 5 nm γ -Al₂O₃ was mixed with the solution to prepare the dispersed suspensions. After overnight equilibration, 2.5 mL of polyphosphate stock solution was added into the prepared suspension. The concentration of metal cations in the filtered supernatant was measured using inductively coupled plasmamass spectroscopy (ICP-MS). All experiments were performed in duplicate. In order to collect good solution and solid NMR spectra with acceptable signal-to-noise ratio, polyphosphate concentrations were set up to 2 mM in total P concentration. This concentration is also similar to the one used in our recent study on enzymatic hydrolysis of polyphosphate, 24 which allows comparison between enzymatic and mineral-catalyzed polyphosphate hydrolysis. A relatively high metal concentration was used to demonstrate their promotion effects on polyphosphate hydrolysis at the γ -Al₂O₃ surface.

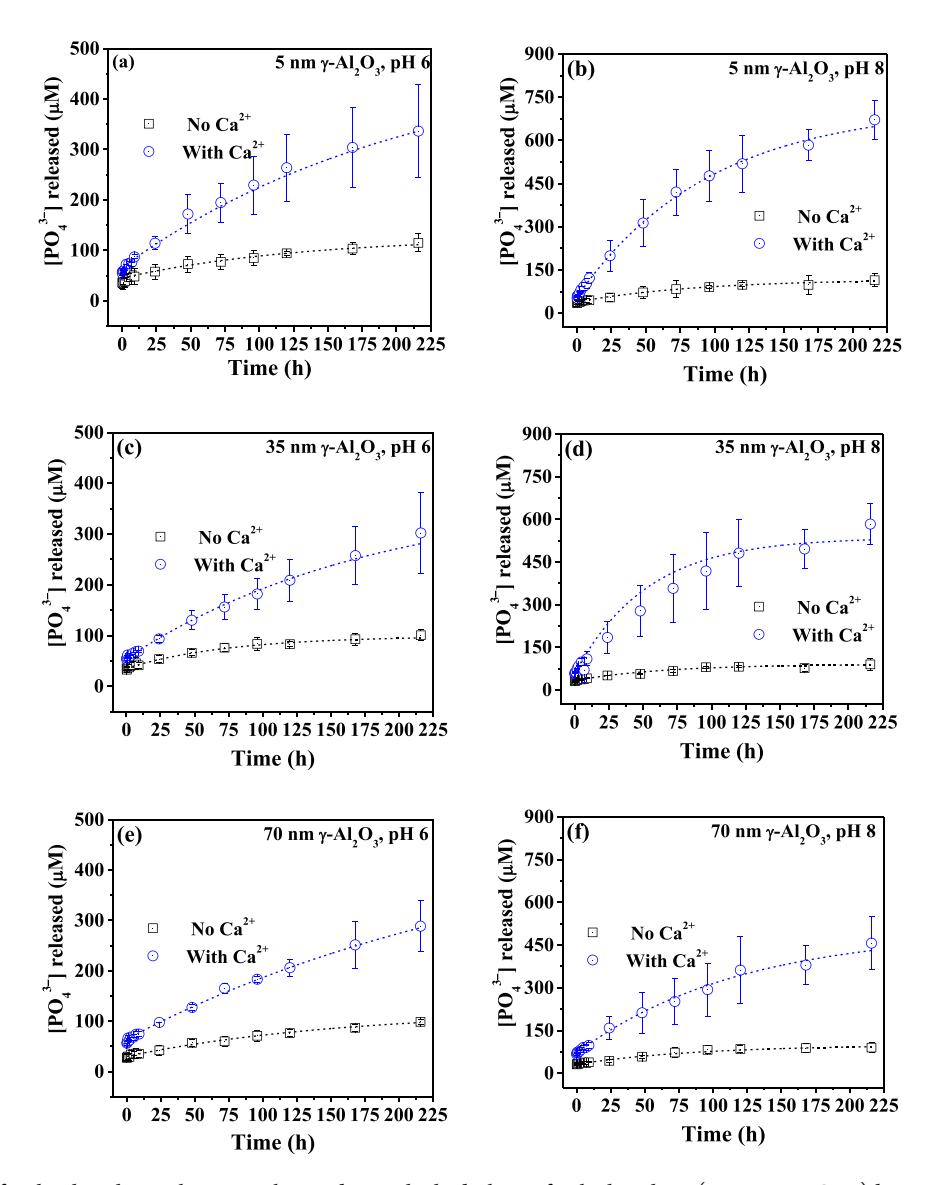


Figure 1. Dynamics of orthophosphate release to solution during the hydrolysis of polyphosphate (Experiment Set I) by 5 nm (a, b), 35 nm (c, d), and 70 nm (e, f) γ -Al₂O₃. Reaction conditions: polyphosphate concentration 2 mM (as total P), pH 6.0 or 8.0, with/without 1 mM CaCl₂. Dashed lines serve as visual guides to represent the trend of orthophosphate release.

2.3. Spectroscopy Analyses. At the end of 216 h (9 d) reaction, the reaction suspensions were centrifuged to separate the solid and supernatant. The supernatant samples were directly used for solution ³¹P NMR analysis. The wet pastes were freeze-dried for solid state ³¹P NMR spectroscopy analyses, including single pulse magic angle spinning (SP/MAS), ³¹P{¹H} cross-polarization MAS (CP/MAS), 2-dimensional (2D) ³¹P{¹H} heteronuclear correlation (HetCor), and ²⁷Al SP/MAS NMR analyses. P K-edge X-ray absorption near edge structure (XANES) spectroscopy analysis was also conducted on the reacted solids following our previous procedure. ²⁴ Details of NMR and XANES data collection and analyses are available in the Supporting Information Text S3—Text S5.

3. RESULTS AND DISCUSSION

3.1. Polyphosphate Adsorption and Hydrolysis on Aluminum Oxides. A previous study showed that γ -Al₂O₃ with different particle sizes had different reactivity for phytate

and orthophosphate sorption, with the sorption capacity for phytate being an order of magnitude higher than that for orthophosphate. 17 Here, we investigated size-dependent adsorption and hydrolysis of polyphosphate by different sized γ-Al₂O₃ in the absence or presence of 1 mM Ca²⁺ (Experimental Set I; Figure 1 and Fig. S4). During the experimental duration, orthophosphate was continuously produced and released into the solution from polyphosphate hydrolysis (Figure 1), and the production rate can be fitted by first-order kinetic model (Fig. S5, Table 1). In the absence of Ca²⁺ and at both pH 6.0 and 8.0, the production rate and extent of orthophosphate was slightly higher for 5 nm γ-Al₂O₃ $(0.19-0.197 \times 10^{-3} \text{ h}^{-1})$ as compared to 35 and 70 nm γ - Al_2O_3 (0.146-0.174 × 10⁻³ h⁻¹). In the presence of 1 mM Ca²⁺, the hydrolysis rate of polyphosphate was obviously improved for all three sized γ -Al₂O₃ (Figure 1 and Fig. S5), roughly following the order of 5 > 35 > 70 nm γ -Al₂O₃, with a 3.5-4.1 times increase at pH 6.0 and a 6.5-10.8 times increase at pH 8.0 (Table 1).

Table 1. First-Order Kinetics Fitting Parameters from Batch Experiments in Figure 1

experimental conditions					
γ-Al ₂ O ₃ particle size (nm)	pН	Ca ²⁺ concentration (mM)	reaction time (h)	$k (10^{-3} h^{-1})$	R^2
5	6.0		216	0.19	0.939
5	6.0	1	216	0.776	0.969
35	6.0		216	0.169	0.919
35	6.0	1	216	0.644	0.995
70	6.0		216	0.174	0.969
70	6.0	1	216	0.605	0.990
5	8.0		216	0.197	0.921
5	8.0	1	216	1.89	0.958
35	8.0		216	0.146	0.888
35	8.0	1	216	1.58	0.948
70	8.0		216	0.167	0.890
70	8.0	1	216	1.08	0.972

The evolution of total dissolved P concentration in the solution (which is the sum of dissolved polyphosphate and orthophosphate) (Fig. S4) is different from the typical features for orthophosphate or organic phosphate adsorption on Fe and Al (hydr)oxides. 12,25 In general, phosphate adsorption on Fe/ Al (oxyhydr)oxides experiences a rapid initial uptake followed by slow uptake, reaching steady state within approximate 5 h. 12,25 In this study, total P concentration in solution decreased quickly within the first few hours and then gradually increased (Fig. S4). The concentration of solution Ca²⁺ at day 9 was significantly lower than that at the beginning of the experiments (Fig. S6), suggesting a large degree of Ca²⁺ immobilization during polyphosphate hydrolysis. We hypothesize that the initial rapid decrease was likely due to the rapid adsorption of polyphosphate onto γ-Al₂O₃ and that the gradual increase of total P concentration over time likely resulted from the hydrolysis of polyphosphate and production of dissolved orthophosphate. We further hypothesize that the change in solution Ca2+ concentration was due to the complexation and precipitation of Ca2+ with polyphosphate and/or produced orthophosphate. These hypotheses were further investigated using solution and solid state ³¹P NMR, as detailed below.

3.2. Solution ³¹P NMR. Since distinctive chemical shifts (δ) can be identified for the NMR spectra of orthophosphate $(\delta_{\rm p} = \sim 1 \text{ ppm})$ and polyphosphate $(\delta_{\rm p} = \sim -9 \text{ ppm} \text{ and } -21)$ ppm for end and middle phosphate groups, respectively), solution ³¹P NMR spectroscopy can be used to evaluate aqueous P speciation during the hydrolysis of polyphosphate.²⁴ Solution ³¹P NMR spectra of polyphosphate supernatant after 9-day reaction with three γ -Al₂O₃ phases are shown in Figure 2. The spectra of the supernatant showed distinctive chemical shifts of orthophosphate and polyphosphate. It also demonstrated the significant enhancement of Ca²⁺ on the hydrolysis of polyphosphate by all three γ -Al₂O₃ at both pH 6.0 and 8.0. In the absence of Ca²⁺, the NMR spectra were dominated by the signal from polyphosphate middle groups, centered at -21.71 ppm (Figure 2). However, in the presence of Ca²⁺, the peak intensity of orthophosphate became a significant component and was similar to that of the polyphosphate end group (Figure 2) or sometimes even stronger, such as during the reaction of polyphosphate with 5 nm γ-Al₂O₃ at pH 8.0 (Figure 2a). Additionally, NMR spectra did not show the random production of shorter chained polyphosphate, which would have resulted in multiple peaks from middle phosphate groups with different chain lengths, as discussed in detail in our recent study.²⁴ This, in combination with the continuous orthophosphate production during batch experiments (Figure 1), suggests that orthophosphate was released one by one from the terminal phosphate groups of polyphosphate molecules, similar to the case of enzyme catalyzed polyphosphate hydrolysis.²⁴ To determine the relative percentage of orthophosphate and polyphosphate in the supernatant, their NMR peaks were integrated and compared. The obtained relative percentage information (based on the ratio of integrated peak areas) was compared to that obtained from wet chemistry analysis (using orthophosphate concentration in Figure 1 and total P concentration in Fig. S4). The calculated results were presented in Table S2. Without Ca2+, polyphosphate was the main P species (>90%) in solution, with 93.6, 94.56, and 94.83% polyphosphate at pH 6.0 and 93.46, 95.07, and 95.31% polyphosphate at pH 8.0 for the supernatants of the 5, 35, 70 nm γ -Al₂O₃ experiments, respectively (Table S2). In the presence of Ca2+, orthophosphate became another main P species and reached 19.33,

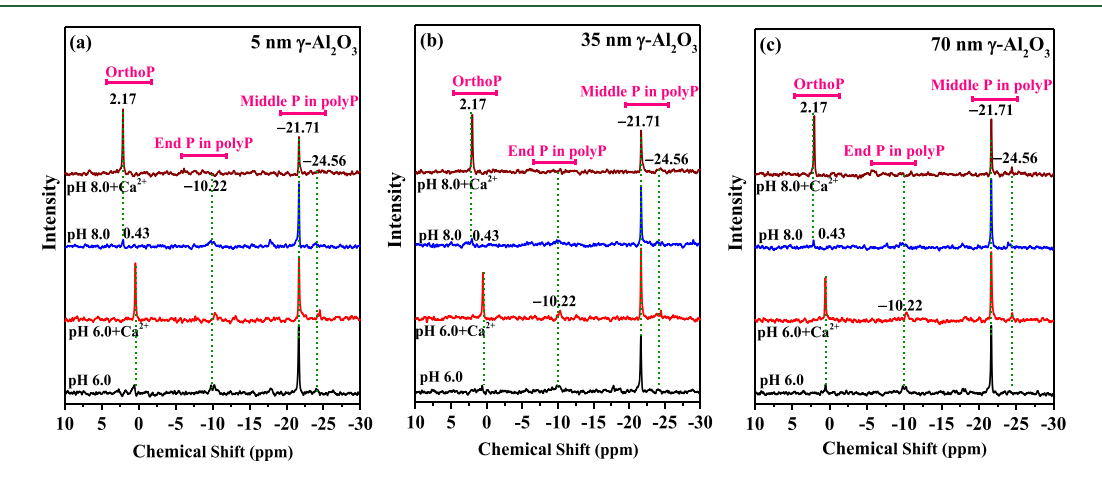


Figure 2. 31 P solution NMR spectra of the liquid supernatant from polyphosphate hydrolysis (Experiment Set I) by 5 nm (a), 35 nm (b), and 70 nm (c) γ -Al₂O₃. Reaction conditions: polyphosphate concentration 2 mM (as total P), pH 6.0 or 8.0, with/without 1 mM CaCl₂, 9 days reaction time.

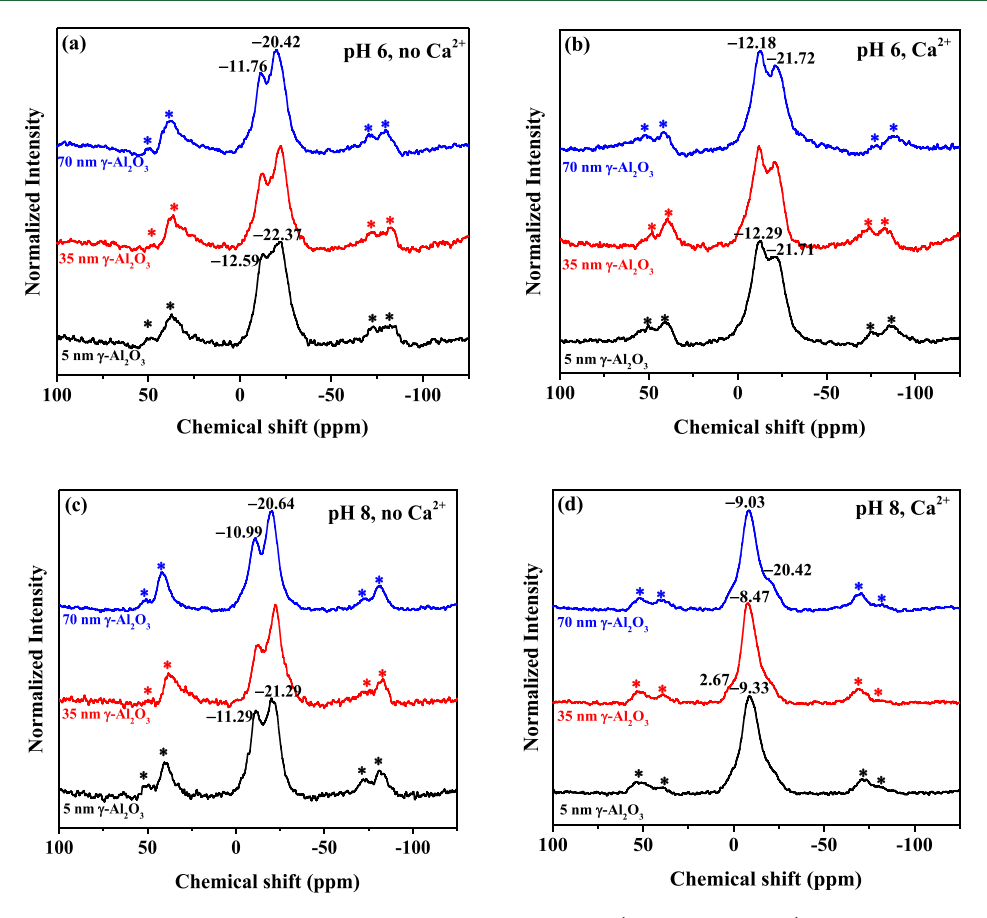


Figure 3. 31 P solid-state NMR spectra of γ-Al₂O₃ reacting with polyphosphate (Experiment Set I). Reaction conditions: polyphosphate concentration 2 mM (as total P), pH 6.0 or 8.0, with/without 1 mM CaCl₂, 9 days reaction time. Asterisks denote spinning side bands.

16.72, and 15.19% at pH 6.0 and 47.49, 35.37, and 26.78% at pH 8.0 for 5, 35, 70 nm γ -Al₂O₃ supernatants, respectively (Table S2). The presence of Ca²⁺ increased the relative percentage of orthophosphate by ~3.5 and 8.5 times for pH 6.0 and 8.0, respectively. Such enhancement is similar to the enhancement observed in kinetic fitting results (Table 1 and Table S2). Overall, these results consistently indicated the ability of Ca²⁺ in enhancing polyphosphate hydrolysis by γ -Al₂O₃.

3.3. Solid State ³¹P SP/MAS NMR. To further elucidate the structure of the solid reaction products, solid state ³¹P NMR analysis was conducted on the freeze-dried solid reaction products. 31P SP/MAS solid state NMR spectra of polyphosphate reacted with γ-Al₂O₃ in the absence/presence of Ca²⁺ for 9 days at pH 6.0 and 8.0 were shown in Figure 3. At pH 6.0 and in the absence of Ca²⁺, spectra of samples with different sized \(\gamma - Al_2 O_3 \) yielded two similar peaks at chemical shifts of around -12 and -21 ppm (Figure 3a). This suggests the presence of similar phosphorus species and similar interaction mechanism(s) between polyphosphate and different sized γ -Al₂O₃. In the presence of Ca²⁺ at pH 6.0, the two peaks at chemical shifts of around -12 and -21 ppm still dominated the NMR spectra but showed different relative intensity as compared to the samples in the absence of Ca²⁺ (Figure 3b). Previous studies showed two NMR peaks at 0 and -6 ppm for orthophosphate adsorption on boehmite¹¹ and two NMR peaks at -1 and -6 ppm for phytate adsorption on γ-Al₂O₃. These peaks were typically attributed to innersphere phosphate surface complexes on Al (oxyhydr)-¹⁷ Specifically, the peaks at \sim -1 and -6 ppm were

assigned to deprotonated bridging bidentate and singly protonated bridging bidentate surface complexes, respectively. 11 In this study, we tentatively assign the phosphate groups in polyphosphate into two categories: those forming direct bonds with the mineral surface (i.e., inner-sphere surface complexes) and those not directly bonded to the mineral surfaces, as schematically illustrated in Fig. S7. These two categories of phosphate groups in polyphosphate molecular are later referred to as polyP-P_{bonded} and polyP-P_{unbonded}. In our study, the chemical shift at ~-21 ppm can be assigned to polyP-P_{unbonded} due to its similarity to the solution NMR signal of middle phosphate groups at \sim -21 ppm (Figure 2). The peak at ~ -12 ppm, close to that of phytate and orthophosphate adsorption at ~ -6 ppm, 11,27 might be attributed to (1) inner-sphere surface complexes between phosphate groups in polyphosphate and mineral surface (i.e., polyP-P_{bonded}), (2) formation of Al polyphosphate/phosphate precipitates, or (3) formation of Ca polyphosphate/phosphate precipitates. Factors 2 and 3 can be eliminated, as discussed below.

For factor 2, the formation of Al phosphate precipitates can result in ^{31}P chemical shift at high field such as aluminum phytate at $\delta_{\rm P}=-11.2~{\rm ppm}^{27}$ and aluminum orthophosphate at $\delta_{\rm P}=\sim\!-10~{\rm ppm}^{.28}$ To rule out the possible formation of aluminum polyphosphate/phosphate precipitates, we measured both solid state ^{31}P and ^{27}Al NMR spectra of these samples as well as a synthetic aluminum polyphosphate standard (Figs. S8 and S9). The ^{31}P chemical shift of aluminum polyphosphate precipitates was at $\delta_{\rm P}=\sim\!-23.55~{\rm ppm}$ (Fig. S8b), far away from the $-12~{\rm ppm}$ chemical shift

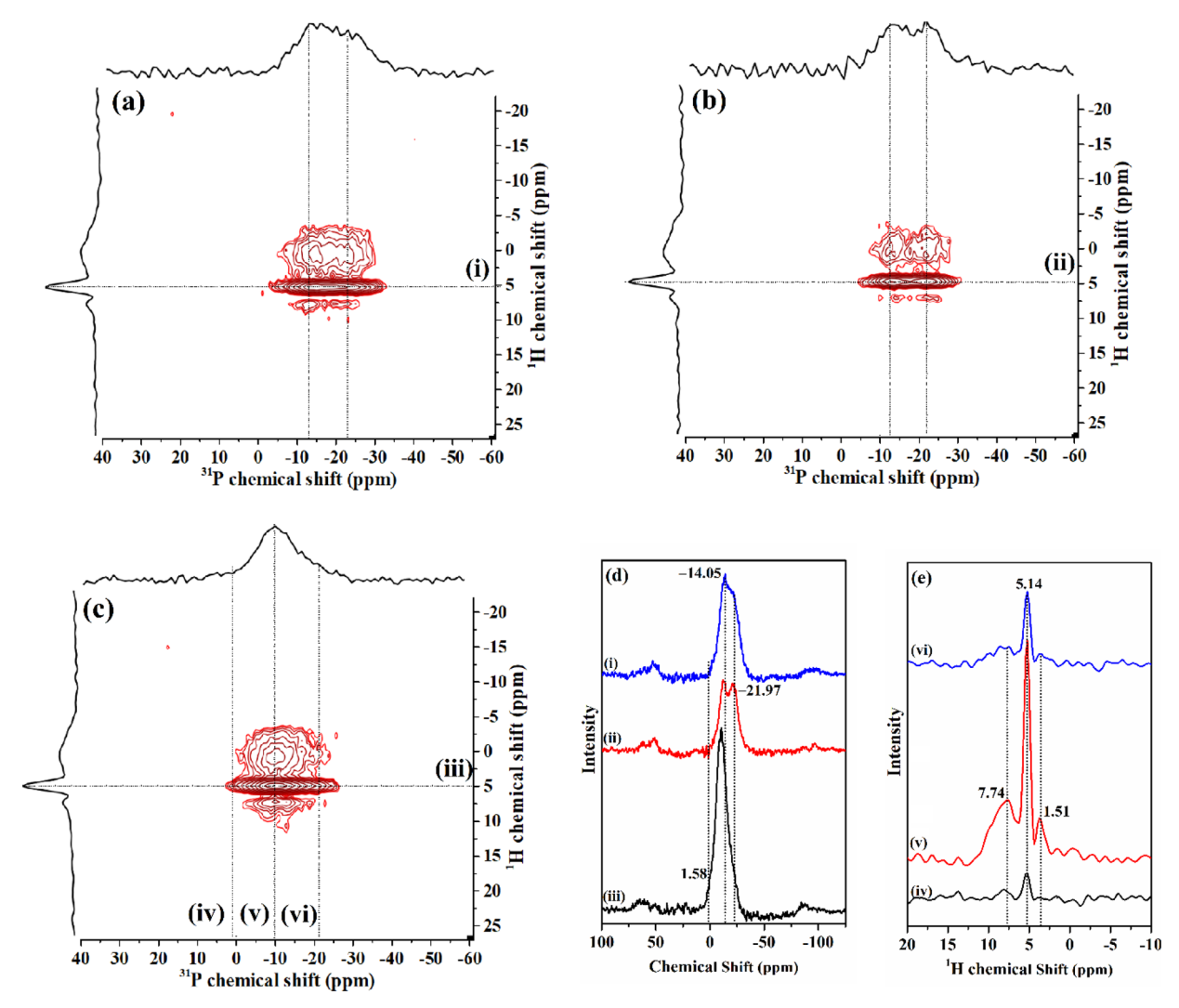


Figure 4. 2D 31 P 1 H} CP-HetCor spectra of the solid reaction products from 5 nm γ -Al $_2$ O $_3$ reacting with polyphosphate (Experiment Set I) at 2 mM polyphosphate (as total P), pH 6.0 or 8.0, with or without 1 mM Ca $^{2+}$, and 9 days reaction time. (a–c) Contour plots for polyphosphate hydrolysis with Ca $^{2+}$ at pH 6.0 (a), without Ca $^{2+}$ at pH 8.0 (b), with Ca $^{2+}$ at pH 8.0 (c), respectively. Spectra on the top and left of the 2D contour plots are sum projections of the 31 P and 1 H dimensions, respectively. (d) Spectra of 31 P cross sections (the F2 dimension) taken at 1 H chemical shifts of 5.14 ppm for the 2D contour maps in parts a–c. (e) Spectra of 1 H cross sections (the F1 dimension) taken at 31 P chemical shifts of 1.28, 10.01, and 20.27 ppm for the 2D contour map in part c.

observed for the reacted samples. In addition, the 27 Al NMR spectrum of aluminum polyphosphate showed one main peak at $\delta_{Al} = -0.29$ ppm and one shoulder peak at $\delta_{Al} = 29.54$ ppm (Fig. S8a). The 27 Al NMR spectra of the reacted samples did not show these peaks at both pH 6.0 and 8.0 (Fig. S9), similar to unreacted γ -Al₂O₃ samples (with two chemical shifts at $\delta_{Al} = \sim$ 65 and \sim 8 ppm). By combining 31 P and 27 Al NMR results, the formation of aluminum phosphate or polyphosphate precipitates can be eliminated as dominant species for the presence of 31 P chemical shift at $\delta_{P} = \sim$ -12 ppm.

For factor 3, the formation of calcium polyphosphate can result in ^{31}P NMR spectra with two peaks at $\delta_P = -9.09$ and -24.13 ppm (Fig. S8b), different from the reacted samples (δ_P at around -12 and -21 ppm). Moreover, after 9-day reaction at pH 6.0, most polyphosphate and orthophosphate remained in the solution (Fig. S4) and were not likely to result in the formation of large amounts of calcium polyphosphate precipitates on the mineral surface. In combination with the similarity of chemical shifts with/without the presence of Ca²⁺

in Figure 3a,b, the formation of calcium polyphosphate should not be the main factor resulting in the ³¹P NMR spectra shape.

Based on the discussion above, the chemical shift at $\delta_P = \sim -12$ ppm can be assigned to factor 1, the formation of polyP-P_{bonded}, i.e., inner-sphere surface complexes (likely as bidentate binuclear complexes) between phosphate groups of polyphosphate and γ -Al₂O₃ surface. The difference in chemical shift (-12 ppm) as compared to orthophosphate or phytate adsorption on aluminum (hydro)oxides (around -6 ppm) li,27 is likely due to the effect of neighboring P atoms in polyphosphate. The bond of bidentate surface complexes with the neighboring phosphate group might lead to the movement of 31P chemical shift toward high field in comparison with the bond with hydrogen atoms. A previous study also indicated that the phosphate tetrahedra in apatite associated with chlorine resulted in the movement of a chemical shift toward high field relative to those associated with fluorine. On the chemical shift toward high field relative to those associated with fluorine.

At pH 8.0 and without Ca^{2+} , the ^{31}P NMR spectra of polyphosphate reacted with γ -Al₂O₃ displayed the same shape

as those at pH 6.0 (Figure 3a,c), indicating the presence of similar species at pH 6.0 and 8.0. However, when Ca²⁺ was present at pH 8.0, the ³¹P NMR spectra showed obvious difference from pH 6.0 samples (Figure 3b,d), with one main peak at around -9 ppm and two shoulder peaks at around 2.67 and -20.5 ppm. The chemical shift at ~ 2.67 ppm belongs to calcium phosphate precipitates, and their crystallinity (amorphous vs crystalline²⁹) will be addressed below in CP dynamic experiments. The chemical shift at \sim -9 ppm can be attributed to phosphate groups of polyphosphate as inner-sphere surface complexes on γ -Al₂O₃ (i.e., polyP-P_{bonded}). The shift of δ_P at around -12 to -9 ppm might be due to the strong chelation between Ca2+ ions and these inner surface complexes (i.e., potential formation of ternary surface complexes and/or precipitates) at high pH (Fig. S6). Fig. S10 showed the Gaussian peak deconvolutions of ³¹P NMR spectra from Figure 3d, and the relative intensities for each resonance line (or corresponding P species) were presented at the bottom of the figures. The relative percentage of calcium phosphate precipitates, phosphate group as inner-sphere surface complexes (i.e., polyP-P_{bonded}), and phosphate group in polyphosphate that were not associated with the mineral surface (i.e., polyP-P_{unbonded}) were at ~10, 70, and 20%, respectively (Fig. S10).

3.4. Two-Dimensional ³¹P{¹H} **CP-HetCor Spectra.** As discussed above, the reacted solids contained phosphate groups in polyphosphate as adsorbed surface complex (i.e., polyP-P_{bonded}), phosphate groups in polyphosphate that were not associated with the mineral surface (i.e., polyP-P_{unbonded}), as well as Ca phosphate precipitates. To further elucidate the protonation and binding state of the phosphate groups as well as the crystallinity of the Ca phosphate precipitates, 2-D solid state ³¹P NMR measurement was performed.

The ³¹P{¹H} CP/MAS NMR spectra (data not shown) of the samples of Figure 3 were similar in chemical shift with their single pulse spectra. Since the ³¹P signal in CP/MAS spectra is transferred from the closest ¹H through the ¹H-³¹P dipolar coupling, the ³¹P signal intensity depends on the ³¹P-¹H distance and numbers of neighboring protons.²⁹ To reveal the protonation of phosphate groups as well as the solid P products (amorphous vs crystalline calcium phosphate precipitates) (Figure 3), a series of CP/MAS solid state ³¹P NMR experiments with variable τ_{CP} values were conducted for three samples (sample information in Fig. S11 caption, fitting methods in Text S4). The CP kinetics can be described using the classical biexponential equation (Text S4), in which intensity increases at short contact times with a time constant $T_{\rm PH}$ and then decreases at longer times with a time constant $T_{1\rho,H}^{31,32}$ T_{PH} relates to the spatial proximity of P to H, and $T_{1\rho,H}$ to the relaxation of the ¹H nuclei.³² For a system with two 1/2 nucleus (in this case ³¹P and ¹H), the heteronuclear dipolar-dipolar interaction is inversely proportional to the internuclear distance and the longer internuclear distance is related to longer $T_{\rm PH}$ and lower CP efficiency.³³ The mobility of the proton sources (e.g., water molecules, surface P-OH and Al-OH groups) also affects the CP efficiency.³³ The buildup of signals at $-16.5 < \delta_{\rm p} < -2$ ppm and $-30 < \delta_{\rm p} <$ -16.5 ppm in the CP/MAS spectra kinetics for all three samples (polyphosphate reacted with 5 nm γ -Al₂O₃ at pH 6.0 and 8.0, with or without 1 mM Ca2+) shows higher CP efficiency, indicating that the main hydrogen species may be P-OH groups derived from the polyP-P_{bonded} and polyP- $P_{unbonded}$ species (Fig. S11a-c).³³ The signal buildup at -2 <

 $\delta_{\rm P}$ < 3.9 ppm in Fig. S11c,d indicated that the formed precipitates of calcium phosphate were in amorphous phase, since (1) amorphous calcium phosphate has a shorter $T_{\rm PH}$ time (0.54 \pm 0.15 ms) with our calculated result of 0.3 ms when compared to crystalline hydroxyapatite (a crystalline Ca phosphate phase) (1.52 \pm 0.08 ms); 32,34 (2) hydroxyapatite would show a significantly slower $^{31}{\rm P}$ NMR signal buildup compared to its amorphous counterparts, and the signal area intensity for hydroxyapatite would decay more slowly with the relaxation time $T_{1\rho,\rm H}$ close to infinity. 29,34,35

We further collected 2-D ³¹P{¹H} HetCor spectra of these three samples in Fig. S11 to distinguish phosphate sites by the nature of associated hydrogen environments, and their 2-D spectra for 3 ms CP time are shown in Figure 4. The spectra in the center of Figure 4a-c were typical 2-D contour plots with the sum projection of the ³¹P dimension on the top and the ¹H sum projection on the left. The ³¹P projection closely resembled their corresponding SP/MAS spectra (Figure 3), and the ¹H projection contained signal only from H atoms near the phosphate. The similarity of the ¹H projection in Figure 4a-c indicated no significant difference of the overall hydrogen environment. Therefore, analysis of the ¹H crosssection spectra at different P chemical shifts was needed. Within the 2-D spectrum of the 5 nm γ -Al₂O₃ sample (reacted with polyphosphate in the presence of Ca²⁺ at pH 6.0) shown in Figure 4a, six different domains were identified. Four domains contained relatively high contour density for the pairs of shifts (δ_H, δ_P) centered at around (1.5 ppm, -14.2 ppm), (1.5 ppm, -22.1 ppm), (5.1 ppm, -14.2 ppm), and (5.1 ppm, -22.1 ppm). Two domains had lower contour density correlating a peak at $\delta_{\rm H}$ = ~7.7 ppm in the $^1{\rm H}$ sum projection with peaks at $\delta_{\rm p}$ = ~ -14.2 and -22.1 ppm in the $^{31}{\rm P}$ projection. The six domains of the 5 nm γ-Al₂O₃ sample prepared without Ca²⁺ addition at pH 8.0 (Figure 4b) showed similar positions as the sample in the presence of Ca²⁺ at pH 6.0, with only differences in contour density (Figure 4a). No contour at $\delta_p = \sim 1.5$ ppm was observed for these two samples. These results indicated that the same coordination environments of hydrogen and phosphorus for surface complexes dominated upon polyphosphate adsorption, due to the lower capability of orthophosphate (produced from polyphosphate hydrolysis, carrying less negative charge as compared to polyphosphate) to compete with polyphosphate for surface adsorption/complexation.

However, the 2-D spectrum of the 5 nm γ -Al₂O₃ sample, reacted with polyphosphate in the presence of Ca2+ at pH 8.0, displayed a different contour shape. The domains at around (1.5 ppm, -9.6 ppm), (5.1 ppm, -9.6 ppm), and (7.7 ppm, –9.6 ppm) dominated the spectrum. For the ^{31}P peak at δ_p = 1.58 ppm, only the ${}^{1}H$ peak at near $\delta_{H} = 5.1$ ppm appeared. The appearance of a ¹H peak at 5.1 ppm in the cross-section of the 1.58 ppm ³¹P peak primarily originated from water molecules and the hydroxyl group of amorphous calcium phosphate, since the existence of crystalline hydroxyapatite is eliminated by CP dynamic results in Fig. S11. 29,34,35 Li et al. (2012) for the first time revealed that boehmite surface catalyzed the crystallization of hydroxyapatite based on the observation of the 2-D HetCor domain in the ^{31}P peak at δ_{P} = 2.65 ppm and the ¹H peak at near $\delta_{\rm H}$ = 0.2 ppm, ²⁹ which did not appear in our 2-D HerCor spectra (Figure 4). The ¹H peak correlated to the surface-adsorbed orthophosphate dominated by restrictedly mobile water in the surface fluid layer could give a relatively narrow peak at $\delta_{\rm H} = \sim 5$ ppm. ³⁶ If the adsorption of

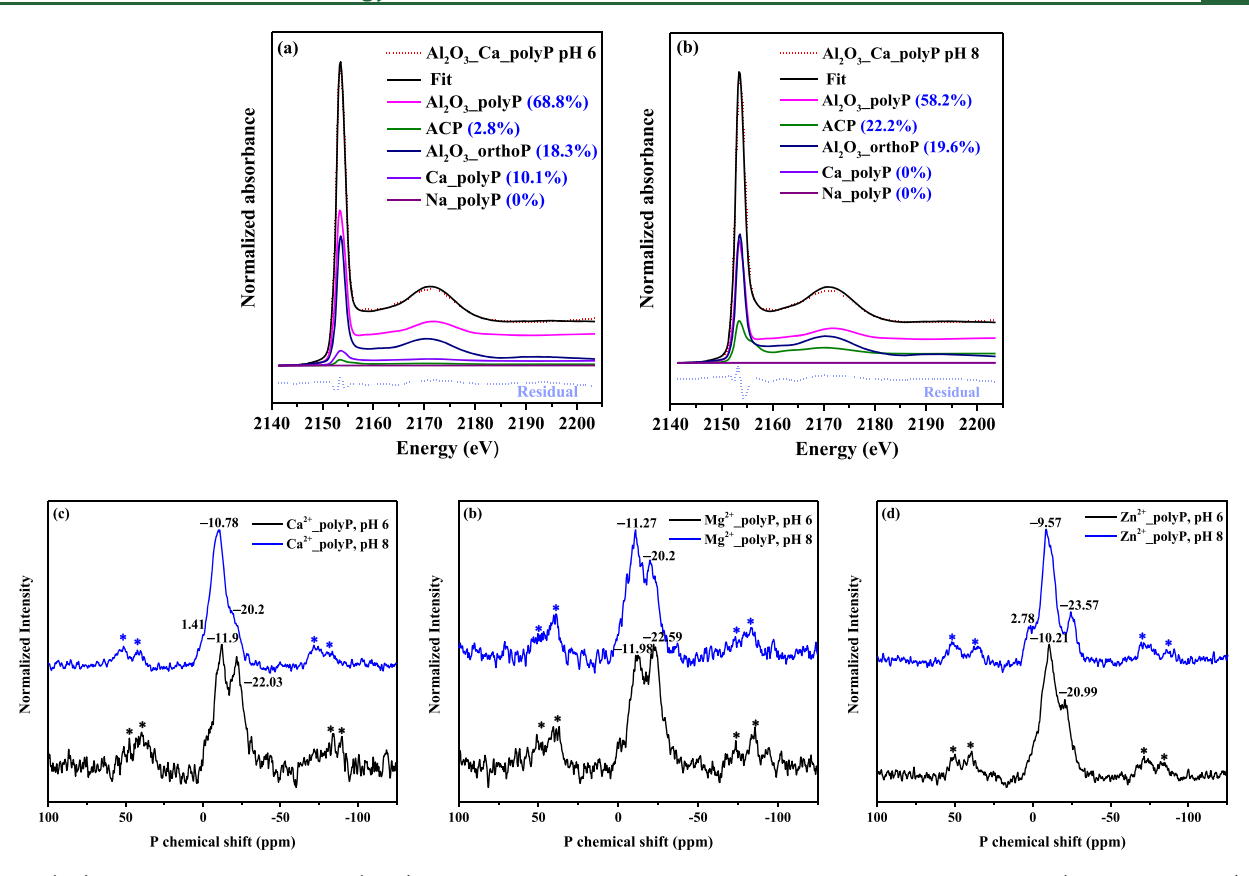


Figure 5. (a,b) Linear combination fitting (LCF) results of P K-edge XANES spectra of the 9-day reaction products (Experiment Set II) from hydrolysis of polyphosphate (1 mM as total P, which is half of the polyphosphate concentration used in Experiment Set I) by 0.1 g/L Al_2O_3 in the presence of 0.5 mM Ca^{2+} at pH 6.0 (a) and 8.0 (b). LCF reference compounds are amorphous calcium polyphosphate (ACP), octacalcium phosphate (octa Ca-orthoP), sodium polyphosphate salt (Na-polyP), calcium polyphosphate precipitates (Ca-polyP), Al_2O_3 -adsorbed polyphosphate (Al_2O_3 -polyP), and Al_2O_3 -adsorbed orthophosphate (Al_2O_3 -orthoP). (c-e) Al_2O_3 -polyP), and Al_2O_3 -adsorbed orthophosphate (Al_2O_3 -orthoP). (c-e) Al_2O_3 -polyP) are total P) at pH 6.0 or 8.0 in the presence of 0.5 mM Al_2O_3 -cd, or Al_2O_3 -cd.

orthophosphate (produced from polyphosphate hydrolysis) could lead to the contour plot in (5.1 ppm, 1.58 ppm), we should observe it in the samples of γ -Al₂O₃ reacted with polyphosphate at pH 6.0 with Ca²⁺ (Figure 4a) and at pH 8.0 without Ca²⁺ (Figure 4b). However, the contour plot in (5.1 ppm, 1.58 ppm) did not appear in Figure 4a,b. After 9-days reaction, approximately half of the total dissolved phosphate remained in the solution as polyphosphate (Table S2), which strongly competed with orthophosphate for surface adsorption sites. Due to the higher negative charge in polyphosphate molecules as compared to orthophosphate, the adsorbed orthophosphate ($\delta_{\rm p} = \sim -3.0$ ppm), in which was not observed in the ³¹P CP/MAS NMR spectra in the ³¹P cross sections (the F2 dimension) taken at ¹H chemical shifts of 5.14 ppm (Figure 4d), should not be a main surface phosphorus species on γ -Al₂O₃. Due to the possible existence of three surface phosphorus species, we chose the spectra of ¹H cross sections (the F1 dimension) taken at ³¹P chemical shifts of 1.58, -10.01, and -20.27 ppm in the sample of Figure 4c and displayed in Figure 4e. Their ¹H NMR spectra did not show obvious differences, indicating that the proton environments mainly came from water molecules or P-OH groups.

3.5. Effect of Metal lons on Polyphosphate Hydrolysis. The effects of common divalent metal cations (Ca²⁺, Mg²⁺, Cu²⁺, Zn²⁺, and Mn²⁺) on polyphosphate hydrolysis were further investigated using 5 nm γ -Al₂O₃ at pH 6.0 and 8.0 (Experimental Set II of Table S1) (Fig. S12). Due to the lowered concentration of polyphosphate, metal cations, and γ -

Al₂O₃ (details in Experimental Set II) compared to those used in the Experimental Set I (Table S1), the hydrolysis extent (Fig. S12a,c) was lower than that those shown in Figure 1 (hydrolysis experiments with/without 1 mM Ca²⁺). Compared to the control experiment (where $4.1 \pm 0.7\%$ polyphosphate was hydrolyzed in the absence of metal cations after 9-days reaction, data not shown), the presence of divalent metal cations all facilitated the hydrolysis of polyphosphate at different degrees. At the same concentration of metal cations (0.5 mM), orthophosphate production followed the order of $Cu^{2+} > Zn^{2+} \approx Ca^{2+} \approx Mn^{2+} > Mg^{2+}$ at pH 6.0 and $Ca^{2+} > Cu^{2+} > Mn^{2+} \geq Zn^{2+} > Mg^{2+}$ at pH 8.0 (Fig. S12a,c). For total P uptake, no significant differences were observed for all metal cations at pH 6.0 (Fig. S12b). At pH 8.0, total P uptake followed the order of $Cu^{2+} > Zn^{2+} \approx Mn^{2+} > Ca^{2+} \approx Mg^{2+}$ (Fig. S12d). Additionally, the uptake of Cu²⁺ and Zn²⁺ was always higher than that of Mn²⁺, Ca²⁺, and Mg²⁺ at both pH values (Fig. S13). The simultaneous decrease of Cu²⁺/Zn²⁺ and total P concentration suggested the potential formation of metal phosphate/polyphosphate precipitates at pH 8.0. Formation of Zn-Al layered double hydroxide at pH 8.0 might be another reason leading to the lowest concentration of Zn²⁺ in the supernatant.³⁷

To investigate P speciation in these systems (5 nm γ -Al₂O₃, presence of five different metal cations), P K-edge XANES and ³¹P solid-state NMR spectroscopy analyses were performed on the freeze-dried reacted solids (Figure 5, Figs. S14 and S15). P

K-edge XANES spectra of samples reacted in the presence of different metal cations did not show a significant difference (Fig. S15). The small peak at 2157.1 eV is likely due to the residual or recrystallized Na-polyphosphate during freezedrying (Fig. S15). To facilitate P XANES analysis, a suite of reference compounds (Fig. S15c, details in Text S5) was used to preform linear combination fitting (LCF) to reveal the possible P species only in the Ca²⁺ system and their relative contributions. For the Ca²⁺ system (Figure 5a,b), fitting results indicated that the main P species in the reacted solids are γ -Al₂O₃-adsorbed polyphosphate and/or orthophosphate as well as amorphous calcium phosphate. Here, due to the spectra similarity between \(\gamma - Al_2 O_2 \)-adsorbed orthophosphate and \(\gamma - \) Al₂O₃-adsorbed polyphosphate (Fig. S15a), the relative percentages of the former from LCF can contain large uncertainty, especially considering the fact that NMR results did not show a significant contribution of γ-Al₂O₃-adsorbed orthophosphate. The percentage of amorphous calcium phosphate became higher at pH 8.0, consistent with the result of solid state NMR spectra (Figure 3).

The solid-state ³¹P NMR spectra of samples reacted in the presence of different metal cations are shown in Figure 5c–e and Fig. S14. Due to the paramagnetic nature of Cu and Mn, NMR measurements of Cu/Mn-containing samples were very challenging and resulted in poor NMR spectra (Fig. S14). In the Mn²⁺ system, no phosphorus chemical shift was observed (Fig. S14b).

For the Ca²⁺ system at pH 8.0, similar to the Ca²⁺ system in Figure 3, the main P species included phosphate groups as inner-sphere surface complexes (i.e., polyP-P_{bonded}) at $\delta_P = -10.78$ ppm, phosphate groups in polyphosphate that were not associated with the mineral surface (i.e., polyP-P_{unbonded}) at $\delta_P = -20.2$ ppm, and calcium phosphate precipitates ($\delta_P = 1.41$ ppm) (Figure 5c). At pH 6.0, it only contained the first two species (Figure 5c).

For the ${\rm Mg}^{2+}$ system (Figure 5d), we observed the phosphate group as inner-sphere surface complexes (polyP-P_{bonded}) at $\delta_{\rm P}=-11.98$ ppm, as well as phosphate groups in polyphosphate that were not associated mineral surface (polyP-P_{unbonded}) at $\delta_{\rm P}=-22.58$ ppm. At pH 8.0, surface complexed phosphate species (polyP-P_{bonded}) became dominant, likely due to ${\rm Mg}^{2+}$ facilitated surface adsorption/complexation of phosphates.

For the Zn²⁺ system (Figure 5e), we observed the presence of zinc phosphate precipitates ($\delta_{\rm P}=2.78~{\rm ppm}$)³⁸ besides innersphere surface phosphate complexes (polyP-P_{bonded}, $\delta_{\rm P}=-10.21~{\rm ppm}$) and phosphate group not associated with mineral surfaces (polyP-P_{unbonded}, $\delta_{\rm P}=-20.99~{\rm ppm}$). We also monitored the structure alteration of γ -Al₂O₃ using ²⁷Al solid-state NMR spectroscopy (Fig. S16). No changes were observed for the γ -Al₂O₃ structure after 9-days reaction in the presence of Ca²⁺, Mg²⁺, Cu²⁺, and Mn²⁺. However, a new shoulder peak at $\delta_{\rm Al}=12.8~{\rm ppm}$ was observed for the Zn²⁺ system (Fig. S16f), suggesting the formation of Zn–Al layered double hydroxide precipitates. ^{19,37}

3.6. Reaction Mechanisms. During the hydrolysis of phosphate monoester by acid or alkaline phosphatase, at the enzyme active site, an intermediate species was formed involving the oxygen atom of the terminal PO_4 group completely coordinated with two metal cations [e.g., Zn(II), Ca(II), Fe(II), Mn(II)]. These metal complexes in phosphatase can initiate double Lewis acid activation for hydrolyzing phosphates by initially bridging the two metal

I

centers with the two phosphoryl oxygen atoms. 42 Purple acid phosphatases can catalyze the hydrolysis of phosphate esters and condense phosphate through a binuclear metal center (diiron Fe-Fe or Fe-Mn/Zn) and produce orthophosphate due to the net transfer of the phosphoryl group to water. 43,44 Based on our results, the phosphatase-mimetic ability of γ-Al₂O₃ toward polyphosphate degradation/hydrolysis likely derives from the ability of Al atoms coordinating with phosphate groups in polyphosphate probably via the formation of bidentate binuclear surface complexes, which activates the P atom for a nucleophilic attack. Surface H₂O and ≡Al-OH, close to the neighboring Al atoms coordinated with phosphoryl O atom, 45,46 might serve as a nucleophilic agent attacking the P atom with a subsequent cleavage of the P-O-P bond, and this ≡Al−OH can be viewed as a reactive center for activating the dissociation of the P-O bond onto γ -Al₂O₃. 46,47

Our observed terminal-only hydrolysis mechanism indicates that one or two terminal phosphate group(s) of polyphosphates can associate with Al atoms at the surface of γ-Al₂O₃ and form bidentate binuclear surface complexes (as schematically illustrated in Fig. S7). Ca2+ and other divalent metal cations can likely coordinate with the surface hydroxyls (≡Al-OH) of γ-Al₂O₃ and/or polyphosphate molecules, forming ternary surface complexes (as previously observed in the presence of phosphate, which can eventually enhance the surface coverage of phosphate). 16,21,48 The difference in hydrolysis extent of five divalent metal cations might be due to their intrinsic affinity to polyphosphate. The order of stability constants of divalent metal cations (except for Mn²⁺, which is not available in the literature) and tripolyphosphate complexes follows $Cu^{2+}(10^{8.01}) > Zn^{2+}(10^{6.55}) > Ca^{2+}(10^{4.98})$ > Mg²⁺ (10^{4.58}).⁴⁹ This is similar to the order of metal cation promotion on polyphosphate hydrolysis at pH 6.0 (Fig. S12a). However, this order was not followed at pH 8.0, likely due to the formation of copper hydroxide precipitates (for Cu²⁺) or Zn-Al layered double hydroxide precipitates (for Zn^{2+}). This was supported by the observation of significant removal of Cu²⁺ and Zn²⁺ from solution. Thus, if not considering Cu²⁺ and Zn²⁺, at pH 8.0, Ca²⁺ has stronger affinity than Mg²⁺ for the promotion for polyphosphate hydrolysis.

4. ENVIRONMENTAL IMPLICATIONS

Polyphosphate adsorption and degradation at the mineralwater interface is of great relevance to the cycling of polyphosphate of natural origin and from human activities. Our laboratory experiments on the hydrolysis of polyphosphate hydrolysis at the mineral-water interface suggested that varied-size γ-Al₂O₃ can promote the hydrolysis of polyphosphate, which is further enhanced in the presence of divalent metal cations. Additionally, at pH 8.0 (similar to seawater pH) and in the presence of Ca2+, continuous hydrolysis of polyphosphate on the surface of γ-Al₂O₃ can lead to the formation of amorphous calcium phosphate precipitates (possibly within days). If the reaction was allowed to proceed for longer term, this might lead to the eventual formation of hydroxyapatite, as was previously observed during long time cosorption of orthophosphate and calcium on boehmite at pH Li et al. (2012) observed the immediate formation of amorphous calcium phosphate precipitates upon mixing orthophosphate and Ca2+ solutions at pH 9.0 in the absence of boehmite, which gradually transformed into hydroxyapatite after 30-day aging.²⁹ In our case, further hydrolysis of polyphosphate may eventually lead to the formation of hydroxyapatite or other crystalline calcium phosphate phases within months at pH 8.0, due to the cosorption of Ca^{2+} and orthophosphate (produced from polyphosphate hydrolysis) on the surface of γ -Al₂O₃ and the aging of the produced amorphous calcium phosphate precipitates.

Overall, our results revealed the critical roles of mineralwater interface reactions and divalent metal cations on controlling polyphosphate degradation and transformation and laid the foundation for better understanding the interfacial geochemical processes governing phosphorus cycling in sediments, soils, and water bodies. Such an abiotically mediated polyphosphate transformation process might offer additional insights for explaining marine sedimentary phosphorus burial via the precipitation of fine-grained apatite particles from exogenous polyphosphate intermediates as previously observed. 4,50,51 Although the concentrations of polyphosphate and metals used in this study are much higher than those in common natural environments, the concentration of Ca²⁺ and Mg²⁺ in seawater (~10 and 50 mM, respectively) are much higher than the concentration used in this study. In marine sediments, calcium polyphosphate granules can also provide local environments with high Ca²⁺ and polyphosphate fluxes.⁴ Additionally, microbial Mn/Fe reduction in soils and sediments may lead to high metal (e.g., Cu, Zn, and Mn) concentrations in the pore-water. 52,53 Future studies might consider exploring the effects of other common environmental minerals (e.g., Fe oxides) and solution conditions (e.g., freshwater vs seawater), as well as comparisons between abiotically (e.g., mineral catalyzed) and biotically (e.g., enzyme) mediated polyphosphate hydrolyses, in order to fully understand the processes affecting the fate of polyphosphate under varied and complex environmental settings.

ASSOCIATED CONTENT

S Supporting Information

The Supporting Information is available free of charge on the ACS Publications website at DOI: 10.1021/acs.est.9b01876.

Texts for characterizations of γ -Al₂O₃ and sodium polyphosphate, experimental setup, and data analysis of ³¹P NMR and P K-edge XANES; Tables for experimental design and solution P composition; Figures for γ -Al₂O₃ TEM images and XRD patterns, plots of orthophosphate, total P and metal concentrations, first-order kinetic fitting, and ³¹P{¹H} CP/MAS NMR kinetics fitting, scheme for polyphosphate coordination, deconvolution of solid NMR spectra, and NMR and XANES spectra of polyphosphate and phosphate references and the reaction products in the metal system (PDF)

AUTHOR INFORMATION

Corresponding Author

*E-mail: yuanzhi.tang@eas.gatech.edu; phone: 404-894-3814. ORCID ®

Yuanzhi Tang: 0000-0002-7741-8646

Present Address

§J.M.D.: Geosciences Research Division, Scripps Institution of Oceanography, University of California San Diego, La Jolla, CA 92093-5004, United States.

Note:

The authors declare no competing financial interest.

ACKNOWLEDGMENTS

This work was supported by the U.S. National Science Foundation (NSF) under Grant Nos. 1559087, 1739884, and 1559124. B.W. thanks the financial support from the China Scholarship Council (CSC) under Grant No. 201606760059. We acknowledge beamline scientist Erik Nelson at SSRL Beamline 14-3 and Johannes Leisen at Georgia Tech NMR Center for help with the experimental setup. Portions of this research were conducted at the Stanford Synchrotron Radiation Lightsource (SSRL). SSRL is a Directorate of SLAC National Accelerator Laboratory and an Office of Science User Facility operated for the U.S. Department of Energy Office of Science by Stanford University.

REFERENCES

- (1) Paytan, A.; McLaughlin, K. The oceanic phosphorus cycle. *Chem. Rev.* 2007, 107, 563–576.
- (2) Rao, N. N.; Gómez-García, M. R.; Kornberg, A. Inorganic polyphosphate: Essential for growth and survival. *Annu. Rev. Biochem.* **2009**, 78, 605–647.
- (3) Kornberg, A.; Rao, N. N.; Ault-Riche, D. Inorganic polyphosphate: A molecule of many functions. *Annu. Rev. Biochem.* **1999**, *68*, 89–125.
- (4) Diaz, J.; Ingall, E.; Benitez-Nelson, C.; Paterson, D.; de Jonge, M. D.; McNulty, I.; Brandes, J. A. Marine polyphosphate: A key player in geologic phosphorus sequestration. *Science* **2008**, *320*, 652–655.
- (5) Diaz, J. M.; Ingall, E. D. Fluorometric quantification of natural inorganic polyphosphate. *Environ. Sci. Technol.* **2010**, *44*, 4665–4671.
- (6) Paytan, A.; Cade-Menun, B. J.; McLaughlin, K.; Faul, K. L. Selective phosphorus regeneration of sinking marine particles: Evidence from ³¹P-NMR. *Mar. Chem.* **2003**, 82, 55–70.
- (7) Martin, P.; Dyhrman, S. T.; Lomas, M. W.; Poulton, N. J.; Van Mooy, B. A. S. Accumulation and enhanced cycling of polyphosphate by Sargasso Sea plankton in response to low phosphorus. *Proc. Natl. Acad. Sci. U. S. A.* **2014**, *111*, 8089–8094.
- (8) Sannigrahi, P.; Ingall, E. Polyphosphates as a source of enhanced P fluxes in marine sediments overlain by anoxic waters: Evidence from ³¹P NMR. *Geochem. Trans.* **2005**, *6*, 52–59.
- (9) Ebuele, V. O.; Santoro, A.; Thoss, V. Phosphorus speciation by ³¹P NMR spectroscopy in bracken (*Pteridiumaquilinum* (L.) Kuhn) and bluebell (*Hyacinthoides non-scripta* (L.) Chouard ex Rothm.) dominated semi-natural upland soil. *Sci. Total Environ.* **2016**, *566*–567, 1318–1328.
- (10) Kulakovskaya, T. V.; Vagabov, V. M.; Kulaev, I. S. Inorganic polyphosphate in industry, agriculture and medicine: Modern state and outlook. *Process Biochem.* **2012**, *47*, 1–10.
- (11) Li, W.; Feng, X.; Yan, Y.; Sparks, D. L.; Phillips, B. L. Solid-state NMR spectroscopic study of phosphate sorption mechanisms on aluminum (hydr)oxides. *Environ. Sci. Technol.* **2013**, 47, 8308–8315.
- (12) Ruttenberg, K. C.; Sulak, D. J. Sorption and desorption of dissolved organic phosphorus onto iron (oxyhydr)oxides in seawater. *Geochim. Cosmochim. Acta* **2011**, *75*, 4095–4112.
- (13) Ruttenberg, K. C. The Global Phosphorus Cycle. In *Treatise on Geochemistry*, 2nd ed.; Turekian, K. K., Ed.; Elsevier: Oxford, U.K., 2014; pp 499–558.
- (14) Arai, Y.; Sparks, D. L. Phosphate reaction dynamics in soils and soil components: A multiscale approach. *Adv. Agron.* **2007**, *94*, 135–179.
- (15) Guan, X. H.; Liu, Q.; Chen, G. H.; Shang, C. Surface complexation of condensed phosphate to aluminum hydroxide: An ATR-FTIR spectroscopic investigation. *J. Colloid Interface Sci.* **2005**, 289, 319–327.

- (16) Inman, M. P.; Beattie, J. K.; Jones, D. R.; Baldwin, D. S. Abiotic hydrolysis of the detergent builder tripolyphosphate by hydrous manganese dioxide. *Water Res.* **2001**, *35*, 1987–1993.
- (17) Yan, Y.; Koopal, L. K.; Li, W.; Zheng, A.; Yang, J.; Liu, F.; Feng, X. Size-dependent sorption of *myo*-inositol hexakisphosphate and orthophosphate on nano—Al₂O₃. *J. Colloid Interface Sci.* **2015**, 451, 85–92.
- (18) Li, W.; Harrington, R.; Tang, Y.; Kubicki, J. D.; Aryanpour, M.; Reeder, R. J.; Parise, J. B.; Phillips, B. L. Differential pair distribution function study of the structure of arsenate adsorbed on nanocrystal-line γ-alumina. *Environ. Sci. Technol.* **2011**, *45*, 9687–9692.
- (19) Li, W.; Livi, K. J. T.; Xu, W.; Siebecker, M. G.; Wang, Y.; Phillips, B. L.; Sparks, D. L. Formation of crystalline Zn-Al layered double hydroxide precipitates on γ -alumina: The role of mineral dissolution. *Environ. Sci. Technol.* **2012**, *46*, 11670–11677.
- (20) Ren, X.; Yang, S.; Tan, X.; Chen, C.; Sheng, G.; Wang, X. Mutual effects of copper and phosphate on their interaction with γ -Al₂O₃: Combined batch macroscopic experiments with DFT calculations. *J. Hazard. Mater.* **2012**, 237–238, 199–208.
- (21) Li, W.; Wang, Y.-J.; Zhu, M.; Fan, T.-T.; Zhou, D.-M.; Phillips, B. L.; Sparks, D. L. Inhibition mechanisms of Zn precipitation on aluminum oxide by glyphosate: A ³¹P NMR and Zn EXAFS study. *Environ. Sci. Technol.* **2013**, 47, 4211–4219.
- (22) Das, P.; Metcalfe, C. D.; Xenopoulos, M. A. Interactive effects of silver nanoparticles and phosphorus on phytoplankton growth in natural waters. *Environ. Sci. Technol.* **2014**, *48*, 4573–4580.
- (23) Murphy, J.; Riley, J. P. A modified single solution method for the determination of phosphate in natural waters. *Anal. Chim. Acta* **1962**, *27*, 31–36.
- (24) Huang, R.; Wan, B.; Hultz, M.; Diaz, J. M.; Tang, Y. Phosphatase-mediated hydrolysis of linear polyphosphates. *Environ. Sci. Technol.* **2018**, 52 (3), 1183–1190.
- (25) Yan, Y. P.; Liu, F.; Li, W.; Liu, F.; Feng, X. H.; Sparks, D. L. Sorption and desorption characteristics of organic phosphates of different structures on aluminum (oxyhydr)oxides. *Eur. J. Soil Sci.* **2014**, *65*, 308–317.
- (26) Huang, R. X.; Tang, Y. Z. Speciation dynamics of phosphorus during (hydro)thermal treatments of seewage sludge. *Environ. Sci. Technol.* **2015**, 49, 14466–14474.
- (27) Yan, Y.; Li, W.; Yang, J.; Zheng, A.; Liu, F.; Feng, X.; Sparks, D. L. Mechanism of *myo*-inositol hexakisphosphate sorption on amorphous aluminum hydroxide: Spectroscopic evidence for rapid surface precipitation. *Environ. Sci. Technol.* **2014**, *48*, 6735–6742.
- (28) Kim, Y.; Kirkpatrick, R. J. An investigation of phosphate adsorbed on aluminum oxyhydroxide and oxide phases by nuclear magnetic resonance. *Eur. J. Soil Sci.* **2004**, *55* (2), 243–251.
- (29) Li, W.; Xu, W.; Parise, J. B.; Phillips, B. L. Formation of hydroxylapatite from co-sorption of phosphate and calcium by boehmite. *Geochim. Cosmochim. Acta* **2012**, 85, 289–301.
- (30) Vaughn, J. S.; Lindsley, D. H.; Nekvasil, H.; Hughes, J. M.; Phillips, B. L. Complex F,Cl apatite solid solution investigated using multinuclear solid-state NMR methods. *J. Phys. Chem. C* **2018**, *122* (1), 530–539.
- (31) Kolodziejski, W.; Klinowski, J. Kinetics of cross-polarization in solid-state NMR: A guide for chemists. *Chem. Rev.* **2002**, *102*, 613–628.
- (32) Mason, H. E.; Montagna, P.; Kubista, L.; Taviani, M.; McCulloch, M.; Phillips, B. L. Phosphate defects and apatite inclusions in coral skeletal aragonite revealed by solid-state NMR spectroscopy. *Geochim. Cosmochim. Acta* **2011**, *75*, 7446–7457.
- (33) Xu, J.; Chen, L.; Zeng, D.; Yang, J.; Zhang, M.; Ye, C.; Deng, F. Crystallization of AlPO₄-5 aluminophosphate molecular sieve prepared in fluoride medium: A multinuclear solid-state NMR study. *J. Phys. Chem. B* **2007**, *111*, 7105–7113.
- (34) Mathew, R.; Gunawidjaja, P. N.; Izquierdo-Barba, I.; Jansson, K.; García, A.; Arcos, D.; Vallet-Regí, M.; Edén, M. Solid-state ³¹P and ¹H NMR investigations of amorphous and crystalline calcium phosphates grown biomimetically from a mesoporous bioactive glass. *J. Phys. Chem. C* **2011**, *115*, 20572–20582.

- (35) Klimavicius, V.; Kareiva, A.; Balevicius, V. Solid-state NMR study of hydroxyapatite containing amorphous phosphate phase and nanostructured hydroxyapatite: Cut-off averaging of CP-MAS kinetics and size profiles of spin clusters. *J. Phys. Chem. C* **2014**, *118*, 28914—28921.
- (36) Li, W.; Feng, J.; Kwon, K. D.; Kubicki, J. D.; Phillips, B. L. Surface speciation of phosphate on boehmite (γ -AlOOH) determined from NMR spectroscopy. *Langmuir* **2010**, 26, 4753–4761.
- (37) Wan, B.; Yan, Y.; Huang, R.; Abdala, D. B.; Liu, F.; Tang, Y.; Tan, W.; Feng, X. Formation of Zn-Al layered double hydroxides (LDH) during the interaction of ZnO nanoparticles (NPs) with γ -Al₂O₃. Sci. Total Environ. **2019**, 650, 1980–1987.
- (38) Roming, M.; Feldmann, C.; Avadhut, Y. S.; der Günne, J. S. a. Characterization of noncrystalline nanomaterials: NMR of zinc phosphate as a case study. *Chem. Mater.* **2008**, *20*, 5787–5795.
- (39) Coleman, J. E. Structure and mechanism of alkaline phosphatase. *Annu. Rev. Biophys. Biomol. Struct.* **1992**, *21*, 441–483.
- (40) Schenk, G.; Elliott, T. W.; Leung, E.; Carrington, L. E.; Mitić, N.; Gahan, L. R.; Guddat, L. W. Crystal structures of a purple acid phosphatase, representing different steps of this enzyme's catalytic cycle. *BMC Struct. Biol.* **2008**, *8*, 6.
- (41) Schenk, G.; Mitić, N.; Gahan, L. R.; Ollis, D. L.; McGeary, R. P.; Guddat, L. W. Binuclear metallohydrolases: Complex mechanistic strategies for a simple chemical reaction. *Acc. Chem. Res.* **2012**, *45*, 1593–1603.
- (42) Williams, N. H.; Takasaki, B.; Wall, M.; Chin, J. Structure and nuclease activity of simple dinuclear metal complexes: Quantitative dissection of the role of metal ions. *Acc. Chem. Res.* **1999**, 32, 485–493
- (43) Schenk, G.; Mitić, N.; Hanson, G. R.; Comba, P. Purple acid phosphatase: A journey into the function and mechanism of a colorful enzyme. *Coord. Chem. Rev.* **2013**, 257, 473–482.
- (44) Huang, X.-L. Hydrolysis of phosphate esters catalyzed by inorganic iron oxide nanoparticles acting as biocatalysts. *Astrobiology* **2018**, *18*, 294–310.
- (45) Mäkie, P.; Persson, P.; Österlund, L. Solar light degradation of trimethyl phosphate and triethyl phosphate on dry and water-precovered hematite and goethite nanoparticles. *J. Phys. Chem. C* **2012**, *116*, 14917–14929.
- (46) Olsson, R.; Giesler, R.; Loring, J. S.; Persson, P. Adsorption, desorption, and surface-promoted hydrolysis of glucose-1-phosphate in aqueous goethite (α -FeOOH) suspensions. *Langmuir* **2010**, *26*, 18760–18770.
- (47) Tan, F.; Zhang, Y.; Wang, J.; Wei, J.; Cai, Y.; Qian, X. An efficient method for dephosphorylation of phosphopeptides by cerium oxide. *J. Mass Spectrom.* **2008**, *43*, 628–632.
- (48) Yan, Y.; Wan, B.; Jaisi, D. P.; Yin, H.; Hu, Z.; Wang, X.; Chen, C.; Liu, F.; Tan, W.; Feng, X. Effects of *myo*-inositol hexakisphosphate on Zn(II) sorption on γ -alumina: A mechanistic study. *ACS Earth Space Chem.* **2018**, *2*, 787–796.
- (49) Maki, H.; Tsujito, M.; Sakurai, M.; Yamada, T.; Nariai, H.; Mizuhata, M. Stabilities of the divalent metal ion complexes of a short-chain polyphosphate anion and its imino derivative. *J. Solution Chem.* **2013**, 42, 2104–2118.
- (50) Goldhammer, T.; Bruchert, V.; Ferdelman, T. G.; Zabel, M. Microbial sequestration of phosphorus in anoxic upwelling sediments. *Nat. Geosci.* **2010**, *3*, 557–561.
- (51) Schulz, H. N.; Schulz, H. D. Large sulfur bacteria and the formation of phosphorite. *Science* **2005**, *307*, 416–418.
- (52) Cooper, D. C.; Picardal, F. F.; Coby, A. J. Interactions between microbial iron reduction and metal geochemistry: Effect of redox cycling on transition metal speciation in iron bearing sediments. *Environ. Sci. Technol.* **2006**, *40*, 1884–1891.
- (53) Müller, B.; Granina, L.; Schaller, T.; Ulrich, A.; Wehrli, B. P, As, Sb, Mo, and other elements in sedimentary Fe/Mn layers of lake baikal. *Environ. Sci. Technol.* **2002**, *36*, 411–420.